The EXODUS incident

Appendix: Technical details

Peter Schattschneider
USTEM facility, TU Wien, A-1040 Vienna, Austria

This Appendix contains the equations and numerical details that are the basis of the surprising phenomena described in the SciFi-novel *The EXODUS incident*. This document is meant to provide the necessary input to the interested reader in order to verify the statements in the novel quantitatively. Some of the following issues can be solved with high school physics, others need a physics bachelor or master level. Many of the fully worked examples given below were used in a university lecture named *How Physics Inspires Science Fiction*. It was great fun for everybody.

Ramjet

The interstellar ramjet, proposed by Robert W. Bussard [1] collects interstellar charged particles (essentially H^+) by some magnetic or electric field configuration. Interestingly, no details on the fields are given in Bussard's original publication. In spite of the fascination that the interstellar ramjet sparked among scholars, proposals for possible field configurations are extremely rare. The community remained shockingly silent, except of an arcane paper [2] presenting a seemingly working solution. On that detail, see the section on magnetic shielding below.

For the moment, let us assume that the scooping of hydrogen fuel works with some future technology. Then the thrust of a reactor is [3]

$$F' = (v' - u')\Phi' = (v' - u')u'\rho' S \tag{1}$$

where u' is the inflow velocity, v' is the exhaust velocity of the flowing medium, and $\Phi' = u'\rho' S$ is the flux of this medium of density ρ' collected over an area S. All primed quantities are measured in the ship's rest frame.

In an inertial reference frame momentarily fixed to the moving ship an observer sees the interstellar hydrogen arriving with the ship's speed $|u'|$. The density ρ_0 of interstellar hydrogen is increased in the ship's est frame by the relativistic Lorentz factor

$$\gamma(u') = \frac{1}{\sqrt{1-(u'/c)^2}}$$

to $\rho' = \gamma(u')\rho_0$. The fusion process delivers energy E to each incoming proton. A portion $\Delta E = E\eta$ is transferred into directional kinetic energy of the exhaust gas where η is the efficiency of this process. This increases the speed of incoming gas particles from u' to the exhaust speed v'. From energy conservation:

$$\gamma(v')m_p\,c^2 = \gamma(u')m_p\,c^2 + \Delta E$$

where m_p is the proton rest mass. Solving this equation gives

$$v' = f(u';\Delta E).$$

The function f is a long, but straightforward expression containing polynomials of up to 4th order.

The ramjet differential equation 1 for the specific thrust F'/S reads now

$$\frac{F'}{S} = (f(u';\Delta E) - u')u'\gamma(u')\rho_0. \tag{2}$$

F', u', v' are functions of time. Assuming a density of interstellar hydrogen [4] of $\rho_0 = 10^6 m_p/m^3$ and an average energy gain per helium ion of 15 MeV, an efficiency $\eta = 0.25$, with $m_p = 1.7 \cdot 10^{-27}$ kg, The Eq. above can be solved numerically, resulting in Fig. 1. Assuming a ship mass of 1500 tons and aiming at a maximum acceleration of $0.1\,g$, a maximum thrust of about two million Newton is needed. This stipulates a sweep radius of $\sim$ 2000 km for funneling the hydrogen.

The ship must have a minimum initial velocity, here $10^{-5}\,c$ for collecting enough hydrogen fuel. This is achieved by conventional boosters and spending fuel from external hydrogen supplies.

The acceleration a' is proportional to the specific thrust. a' increases first because more hydrogen is scooped with increasing velocity, but later on it decreases because the relativistic mass of the inflow protons increases which makes

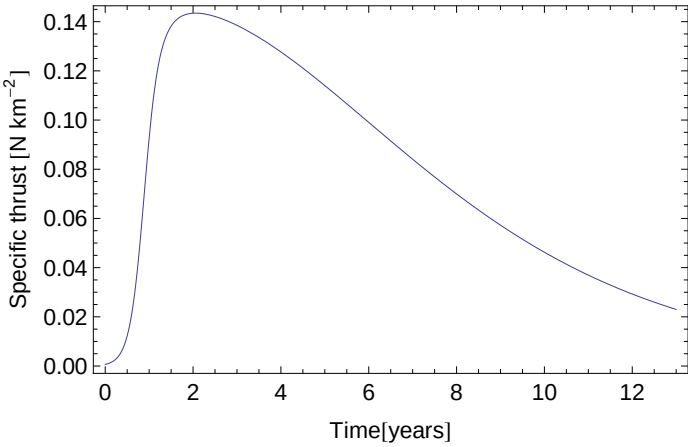

Figure 1: Thrust of the ramjet reactor per square km scooping as a function of time when permanently burning. For comparison, the first stage of the Saturn V rocket delivered a thrust of $\sim$ 35 MNewton.

it less efficient to increase the momentum of the exhaust gas. (Seen from Earth, the acceleration decreases because the ship's mass increases with speed.)

The speed is bound by c as it must be, reaching 80 % of the light speed when passing Proxima Centauri after $\sim$ 10 years under permanent acceleration. However, the ship must start to break at halfway which is reached at $\sim$ 7 years travel time.

For breaking, thrust inversion is used by switching off the reactor and blocking the funnel exhaust. The momentum of the hydrogen repelled by the magnetic field is transferred to the ship. It is similar to breaking by air drag. It can be kept at 0.1 g by tuning the magnetic field strength of the funnel. Only close to destination the fusion reactor must be reactivated for additional thrust inversion. It should be noted that for the time being, no magnetic field configuration is known that could harvest sufficient amounts of hydrogen. A proposal by Fishback [2] works theoretically, but needs prohibitively long solenoids [5].

Electron stripper

One to two thirds of interstellar hydrogen is neutral [4]. For magnetic scooping it must be ionized beforehand. A foil stripper, as used in particle accelerators, e.g. [6] charges the atoms. The process is based on charge exchange in thin films, often carbon, graphene or nanotube foils [7]. For the EXODUS starship

an advanced version consisting of a carbon nanotube forest is used, in order to enhance the efficiency. The thin sheet is positively charged. For a bias voltage of 1 kV, the electric field at the tips of nanotubes of 2 nm diameter is extremely strong, $\sim 10^{12}$ V/m, largely surpassing the threshold for field ionisation of hydrogen [8], $F_c = 3.6 \cdot 10^{10}$ V/m. Similar to ion thrusters, the electrons extracted from the gas by the stripper anode are reinjected into the pipeline so as to obtain a hydrogen plasma flow towards the fusion drive.

Drag

Assuming that a magnetic funnel can collect ions into the axial pipeline like a lens collects light into a narrow glass fiber, there seems to be no drag force because the speed of particles in a magnetic field is constant. This is wrong because ions perform cyclotron motion around field lines, so their velocity vector in a high magnetic field (close to the pipeline entrance) is almost perpendicular to the flight direction. Averaged over a cyclotron period, their linear momentum is very small; the largest part was transmitted to the magnetic field and thus exerts a drag force on the ship. It has been proposed to slow the ions down in an electrostatic field before they are fed into the reactor, and re-accelerating the exhaust plasma in a tandem capacitor [9].

Fusion

the p-p reaction

$$p + p \rightarrow {}^2D + e^+ + \nu$$

has a very low cross section, 24 orders of magnitude smaller than the main process used in fusion reactors with deuterium

$$\begin{aligned} {}^2D + {}^2D &\rightarrow {}^3He + n \\ {}^2D + {}^2D &\rightarrow T + p. \end{aligned}$$

Whitmire [9] proposes a catalytic reaction based on the CNO-(or Bethe-Weizsäcker) cycle [10] that takes place in hot main sequence stars.

$$\begin{aligned} {}^{12}C + p &\rightarrow {}^{13}N + \gamma \\ {}^{13}N + p &\rightarrow {}^{14}O + \gamma \\ {}^{14}O &\rightarrow {}^{14}N + e^{+} + \gamma \\ {}^{14}N + p &\rightarrow {}^{15}O + \gamma \\ {}^{15}O &\rightarrow {}^{1}5N + e^{+} + \gamma \\ {}^{15}N + p &\rightarrow {}^{12}C + \alpha. \end{aligned}$$

These reactions are 10^{18} times faster than the p-p reaction and can be used as a catalytic fusion process because C, N and O are not depleted in the cycle. At maximum speed, the scooped hydrogen is equivalent to a proton flux of $dN/dt \sim 2 \cdot 10^{27}$ particles/s into the pipeline. They must go through the CNO cycle. At a proton number density of $n_p = 5.10^{25}$ m^{-3} in the fusion chamber and an average burning rate of $\langle \sigma v \rangle = 2.10^{-28}\, m^3 s^{-1}$ that means [9]

$$\frac{dN}{dt} = n_p n_N \langle \sigma v \rangle V$$

with $n_N = n_p$, the density of the Nitrogen catalyst, wherefrom the volume V of the fusion chamber is obtained. For the *EXODUS* this corresponds to a spherical reactor of 11 m radius. The total mass of the catalyst (C, N, O) in the fusion chamber amounts to less than 10^{10} Nitrogen atoms, that is 10^{-10} milligram.

Space Travel

Relativistic equations

Calculations of the starship's trajectory, time delays of radio/laser signals and relativistic effects were based on the equations of special relativity [11]. Henceforth the speed of light in vacuum is set to $c = 1$, the units of space and time are then light year and year. v is the velocity of the ship in earth's inertial frame S. An object moving with u seen from earth moves with

$$u' = \frac{u - v}{1 - uv}$$

seen from the ship. After some algebra the acceleration of an object moving with u' on the ship is

$$a' := \frac{du'}{d\tau} = \frac{du'}{du}\frac{du}{d\tau} = \frac{1-v^2}{(1-uv)^2}\frac{du}{d\tau}$$

where t is time in the inertial frame S of earth, and τ is proper time measured on the ship. This equation was used for programming a freely falling object on the ship. It serves to determine the acceleration, mimicking an accelerometer. Its starting velocity in the ship's frame is $u' = 0$, so $u = v$, and

$$a' = \frac{1}{1-v^2}\frac{du}{d\tau} = \gamma^2\frac{du}{d\tau},$$

or

$$\frac{du}{d\tau} = a'\gamma^{-2} \tag{3}$$

where $\gamma = \gamma(u) = 1/\sqrt{1-u^2}$. We may now define the proper acceleration

$$a := \frac{du}{d\tau}$$

where $u = dx'/d\tau = dx/dt$ is the (relative) speed of the ship's environment, i.e. the speed of the receding earth seen from the ship which is identical with the speed of the ship seen from earth. For constant a', this gives the well-known expressions

$$u = \tanh(a'\tau),$$

$$\gamma = \cosh(a'\tau),$$

$$t = \frac{1}{a'}\sinh(a'\tau),$$

$$x = \frac{1}{a'}\cosh(a'\tau).$$

Worldlines of objects uniformly accelerated in their rest frame are therefore hyperbolae

$$x^2 - t^2 = (1/a')^2.$$

For variable acceleration $a' = a'(\tau)$, we separate the variables in Eq. 3 as

$$\gamma^2\, du = a'(\tau)\, d\tau$$

and integrate both sides:

$$\int a'(\tau)d\tau = \frac{1}{2}(\log(1+u) - \log(1-u)) = \operatorname{arctanh}(u)$$

or

$$u(\tau) = \tanh[\int_0^\tau a'(\tau')d\tau']. \tag{4}$$

Knowing $\alpha'(\tau)$, with $dt/d\tau = \gamma, \quad dx/d\tau = dx/dt\, dt/d\tau = u\gamma$ we obtain the space-time trajectory of the ship as a function of the ship time τ which serves as a curve parameter:

$$\begin{aligned} x(\tau) &= \textstyle\int_0^\tau u(\tau')\gamma(u(\tau'))\, d\tau' \\ t(\tau) &= \textstyle\int_0^\tau \gamma(u(\tau'))\, d\tau' \end{aligned} \tag{5}$$

Eqs. 4, 5 were used to calculate the world line $x(\tau), t(\tau)$ of the spaceship in the inertial reference frame S of an observer on earth. Also the relativistic time dilation (*slip correction*) displayed on the belt monitor

$$\text{slip correction} = t - \tau$$

that describes the twin paradox effect, was thus calculated. As input for the computations, the acceleration $a'(\tau)$ - Eq. 2 - was used.

Although scholars [12, 13] do not agree on the derivation of time dilation in rotating reference frames (Einstein himself thought that the centrifugal force on a rotating platform distorts spacetime, but this causes a paradox as shown by Ehrenfest [14], there is general consensus that to first order the time τ measured in a rotating frame relates to time t in an inertial system which is at rest with the axis of rotation is

$$\tau = \sqrt{1 - \frac{\omega^2 r^2}{c^2}}t, \tag{6}$$

where ω is the angular velocity of the rotating reference frame, and r is the distance from the axis. Replacing the centrifugal acceleration $\omega^2 r$ with the gravitational acceleration GM/r^2, where G is the gravitational constant, the equation is formally identical with the time dilation in a gravity potential of a central mass M

$$\tau = \sqrt{1 - \frac{MGr}{c^2}}t. \tag{7}$$

Inserting the values ($\omega = 0.25$ rad/s, $r = 141$ m at level 4) the centrifugal acceleration is 0.9 g, and one arrives at a relativistic time delay of the same order of magnitude as on earth, where it must be considered in GPS systems. It amounts to 0.21 μs/year.

Construction

Artificial gravity

The construction takes care that still standing persons always stand on a horizontal surface. The condition is that the centrifugal acceleration $\mathbf{b} = (r\omega^2, a')$ is always perpendicular to the tangent $\mathbf{t} = (dr, dz)$ of the curved surface, that is $\mathbf{b} \cdot \mathbf{t} = 0$ or

$$r\, dr\omega^2 + a' dz = 0,$$

or

$$\frac{d}{dz} r^2 = -2a'/\omega^2$$

with boundary condition $r = 0$ at $z = 0$. It can be immediately integrated. Since $a' < 0$,

$$r^2 = \frac{2|a'|}{\omega^2} z, \tag{8}$$

defining a parabola with axis z, the flight direction. The equation was solved for an angular frequency of $\omega = 0.25$ rad/s.

Atmospheric pressure

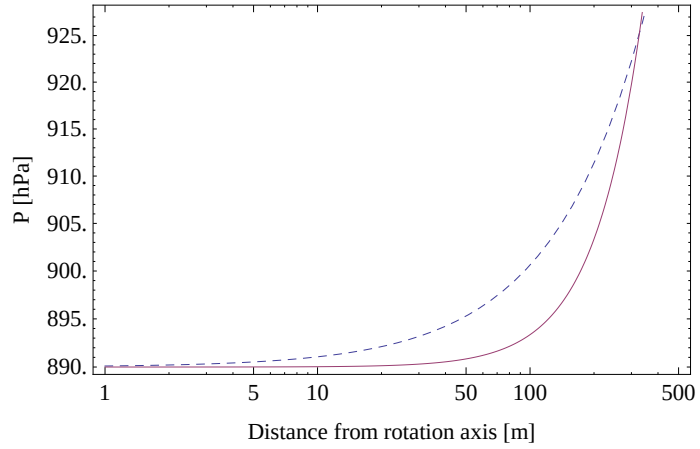

Figure 2: Atmospheric pressure on the spaceship. Dashed: Original version with barometric height equation

An earth like atmosphere at a pressure of 890 Hektopascal was simulated, corresponding to a standard pressure at 1000 m over sea level, according to the

barometric height equation

$$p(r) = p_0\, e^{rgM/RT}$$

where g is (earth's) gravity, M is the molar mass of air, R is the gas constant, and T the temperature in degrees Kelvin. In a rotating environment g must be replaced by the artificial gravity r/ω^2, with the angular rotation frequency ω of the module so

$$p(r) = p_0\, e^{r^2\omega^2 M/RT}.$$

Fig. 2 compares the pressure when descending from the axis with that on earth (starting at 1000 m above sea level). Up to an axial distance of 330 m the pressure increase is below that on earth. The pressure differences within the belt are less than 1 hPa whereas the earth like atmosphere would show 5 hPa.

The dimensionless Rossby number

$$\mathrm{Ro} = \frac{v}{2L\omega}$$

where v is the characteristic velocity of winds, L is a characteristic length of the atmospheric phenomenon, and ω the angular frequency of the ship's rotation, gives a quick estimate whether circulating atmospheric cells can occur. At intrinsically low wind speeds of a few km/h and $\omega = 2\pi/25$ s^{-1}, the Rossby number for the belt ($L = 50$ m) is Ro ~ 0.1, similar to low pressure systems on Earth. Thus, circulating cells are expected. They were simulated with a finite element code [15].

Coriolis trajectories

Trajectories of freely falling objects were calculated as straight lines in a non-rotating reference frame with initial conditions $\vec{x}(t = 0) = \vec{x}_0$, $\vec{v}(t = 0) = \vec{v}_0$, and transformed into the rotating paraboloid. As an example, Fig. 3 shows trajectories for a starting velocity of 40 km/h for a number of throwing directions.

GCR shielding

At the maximum speed of 0.56 c, protons hit the ship's bow with a kinetic energy of 194 MeV. The stopping power — energy loss E per unit path length

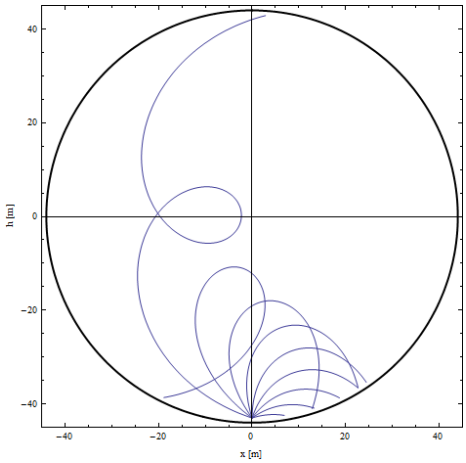

Figure 3: Freely falling objects for a starting speed of 40 km/h, thrown into different directions.

x — $dE/dx = f(E)$ in water is well documented, e.g. [16]. After the separation of variables

$$\frac{dE}{f(E)} = dx$$

the differential equation can be easily solved as

$$x(E) = \int_{E}^{E_0} |f(E)|^{-1}\, dE.$$

This function peaks at the maximum penetration depth which in the present case is 24.5 cm where all protons come to a halt. Since the slowing down is a stochastic process the sharply peaked curve must be convolved with an appropriate broadening function such as a Gaussian, here with a FWHM of 1.5 cm.

Weaponry

Destruction of JIAN TOU

The relative speed between the two space ships is 0.15 c. The ejection speed of the Al bullets is $v_b = 3$ km/s. (As of 2020, the speed record for electromagnetic launch systems is 2.4 km/h, equivalent to the escape velocity from the moon [17]). The distance to the JIAN TOU at its closest approach is $d_{min} = 10^4$ km. Leading the target by 45 degrees, the time to impact is

$$t = \frac{d_{min}}{v_b \sin(\pi/4)} = 4700\, s.$$

The impact occurs at a distance of 14 000 km. The EXODUS passes JIAN TOU 0.22 seconds later at its closest approach.

Leading the target at 90 degrees minimizes the time to impact (in the example, it is shorter by a factor of $\sin(\pi/4)/\sin(\pi/2) = 1/\sqrt{2}$). Arguments favoring a lead angle towards the flight direction in order to hit the target earlier are wrong.

At a speed of 0.15 c, a spherical Al bullet of 200 mm diameter has a kinetic energy equivalent to 2300 kilotons TNT explosive power, almost 200 times the energy of the Hiroshima bomb.

Astrophysics

The description of the sky from destination, looking towards Sol, was simulated with Celestia.

Geometric aberration of the star field

The relativistic aberration of star positions [18] was implemented as

$$\cos\theta = \frac{\cos(\theta_0) - \beta}{1 - \beta\cos(\theta_0)}.$$

By aberration, the star field is contracted around the forward flight direction, and stars are brighter there than for an observer at rest, also known as beaming effect (see Doppler effect below). At the ship's maximum speed of 0.56 c the aberration is almost linear up to 50 degrees viewing angle as shown in Fig. 4, stars appear at roughly half the angle (measured from the forward direction) than for an observer at rest. That means, in front view the star field is compressed, whereas in rear view it is thinned out.

Doppler effect

The Doppler effect changes the frequency of starlight arriving at viewing angle θ, measured with respect to flight direction, as

$$\nu' = \frac{\nu}{\gamma(1 - \beta\cos\theta)}. \tag{9}$$

$\beta = |v|/c$, and $\gamma = 1/\sqrt{1-\beta^2}$ is the relativistic factor. This changes the color of stars seen from the ship - to the blue when viewing into flight direction ($\theta = 0$),

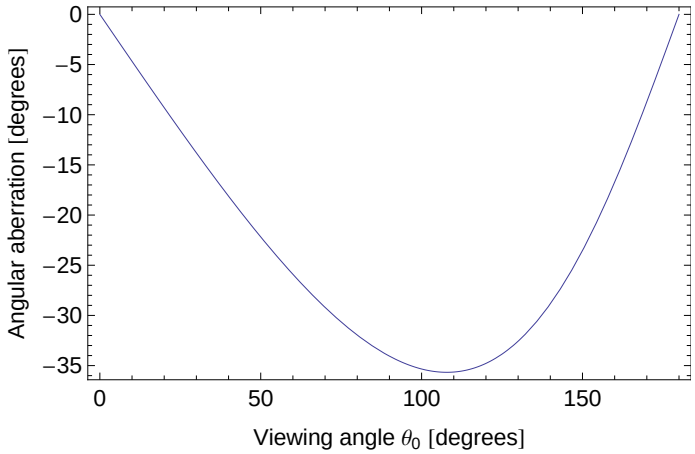

Figure 4: Angular aberration of stars seen from the ship at maximum speed of 0.56 c.

and to the red in rear view. To a good approximation, stars emit black body radiation

$$P \propto \nu^3 \frac{1}{e^{h\nu/kT} - 1} \tag{10}$$

Here, T is the temperature of the emitting body, and h, k are Planck's and Boltzmann's constants. Inserting Eq. 9 into Planck's Eq. 10 it is evident that the Doppler shift changes the apparent temperature T of a star to

$$T' = T/\gamma(1 - \beta\cos\theta) \tag{11}$$

as a function of the ship's speed $v = \beta c$ and the viewing angle θ. γ is the relativistic factor. In the CIE color space, black bodies of temperature T lie along a line called *Planckian locus*. At maximal speed of 0.56 c, for Sol in rear view, inserting the surface temperature of a G-class star of 5800 K, the apparent temperature becomes 3100 K, slightly cooler than Antares, the orange-reddish star in the constellation of Scorpius. In flight direction, Proxima Centauri with a surface temperature of 3000 K appears as a star of 5600 K, yellow as our Sun. The radiant emittance of a body is $P \propto \sigma T^4$, according to the Stefan-Boltzmann law. With Eq. 11

$$\frac{P}{P'} = \gamma^4(1 - \beta\cos\theta)^4$$

the change in brightness of a star according to the Doppler effect can be calculated.

The translation of emittance change to stellar magnitudes is based on the magnitude definition: an emittance increase by a factor of 2.5 corresponds to one magnitude.

Terrell rotation

Assume an object of size R moving at relativistic speed with respect to the observer in positive x direction. The observer is at $y \gg R$ We look at the object at closest distance of the fly-by. When simulating instantaneous images ("snapshots"'), the relativistic Lorentz contraction must be supplemented by the run time difference of light coming from parts of the object at different distances y to the observer. In order that all light rays arrive at the observer at the same time:

$$x' = x/\gamma - \beta y. \tag{12}$$

For $\beta = 0.156$, the deviation of the Lorentz contracted ellipsoid from a sphere is 1.5 % and invisible for the naked eye. For $\beta = 0.9$, the effect is much stronger. The situation is depicted for a sphere in Fig.5. The Lorentz contracted sphere

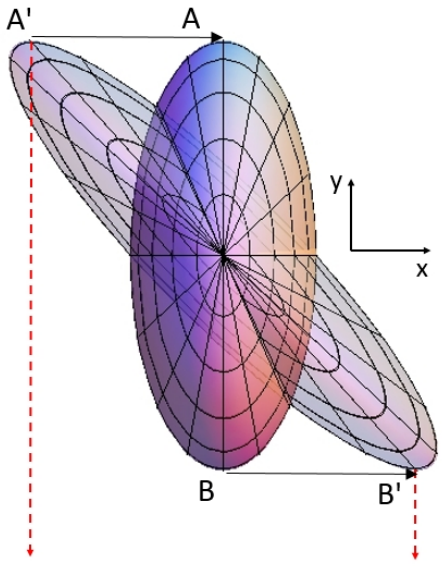

Figure 5: Terrell effect: A sphere moving at 0.9 c from left to right. Light rays (red dashed) travel to a distant observer at the bottom of the page. The more distant point A is seen at an earlier time (A'), the nearer point B at a later time (B').

moves from left to right, the observer is far away at the bottom of the page. The

image shows the moving sphere from above the north pole with the different run time of light from the surface points of the sphere to the observer, Eq. 12 taken into account. The projection for the distant observer is again a sphere, and the Lorentz ellipsoid appears rotated.

Einstein thought that the Lorentz contraction could be "'seen"'. That this is not the case was first mentioned by James Terrell in 1957 and published two years later [19]. Roger Penrose and others have also published on the subject.

Diurnal cycle of Proxima

The semi major axis of the orbit is 0.0485 AU. The numerical eccentricity $\epsilon = 0.11$. This leads to a strong anomaly [20] (periodic east-west oscillation of Proxima on the sky). Superimposed is a south-north seasonal motion because the rotation axis of the planet is inclined by 15 degrees to the pole of the ecliptic. The planet has a tidally bound rotation with periodicity of one stellar year (269 hours). The Equation of the Center (*Mittelpunktsgleichung, J. Kepler 1609*)

$$\Delta\alpha = (2\epsilon - \frac{\epsilon^3}{4})\sin(\alpha)$$

yields the true anomaly $\Delta\alpha$ as a function of the angular position α of a reference object on a circular orbit with the same long axis where $\alpha = 2\pi t/T$ and t, T are time and orbital period. The true anomaly is the angular deviation of the central star on the sky from a hypothetical star in a circular orbit at the same time. It causes a periodic oscillation of the object over the hypothetical star in the ecliptic plane. This oscillation must be transformed into the equatorial coordinate system of the planet with tilted axis (here 15 degrees with respect to the ecliptic pole) and superimposed with the rotation of the planet. We perform the transformation of points P between coordinate systems with rotation operators by an angle δ over a rotation axis with unit vector $\vec{r}$ given in spherical coordinates $\vec{r} = \{\theta, \phi, r = 1\}$:

$$R_{\vec{r}}(\delta) = e^{i\frac{\delta}{2}\vec{r}\cdot\vec{\sigma}} = \cos(\delta/2)\mathbb{1} - i\sin(\delta/2)\vec{r}\cdot\vec{\sigma}$$

where $\vec{\sigma} = \{X, Y, Z\}$ is the 3D-vector of Pauli matrices

$$\begin{aligned} X &= \begin{bmatrix} 0 & 1 \\ 1 & 0 \end{bmatrix} \\ Y &= \begin{bmatrix} 0 & -i \\ i & 0 \end{bmatrix} \\ Z &= \begin{bmatrix} 1 & 0 \\ 0 & -1 \end{bmatrix}, \end{aligned}$$

and $\mathbb{1}$ is the unity matrix. (This formalism is widely used in quantum mechanics, especially for the manipulation of qubits.) Points on the (Bloch) sphere transform as

$$P' = R_{\vec{r}}(\delta) \cdot P,$$

where the rotation axis $\vec{r}$ is the orientation of the equinox, which we fix in x direction: $\vec{r} = \{1, 0, 0\}$, and $\delta = 15$ degrees. The ecliptic longitude of the periastron is assumed to be 103 degrees as for the earth orbit. The apparent track of Proxima on the sky can then be visualized for any position on the planet, again by another rotation operation. Seen from the landing site Cape Cod, Proxima tracks a tilted, almost circular loop on the western horizon. Fig. 6 compares it with what we would see on earth were she tidally locked to the sun (dashed line). The dotted line refers to a circular earth orbit - the yearly north-south oscillation is transformed into a self-crossing loop due to the transformation from ecliptic to equatorial coordinates.

The angular size of Proxima on the sky of Atlantis is D/d where $D = 107000$ km is the diameter of Proxima (or 0.154 diameters of our sun) and $d = 0.0485$ A.U. is the distance to Proxima. The result is 3.17 times the angular appearance of the sun on earth or 1.6 degrees. According to the eccentricity $\epsilon = f/a$ where f is the distance of the focus from the center of the ellipse, and a is the half long axis, Atlantis is closer to Proxima in summer than in winter, with a distance $d = a(1 \mp \epsilon)$. Accordingly, Proxima's size in the sky varies by $\mp 11\%$.

The luminosity of a star of surface area A and absolute temperature T is given by Stefan-Boltzmann's law,

$$L = A\,\sigma T^4$$

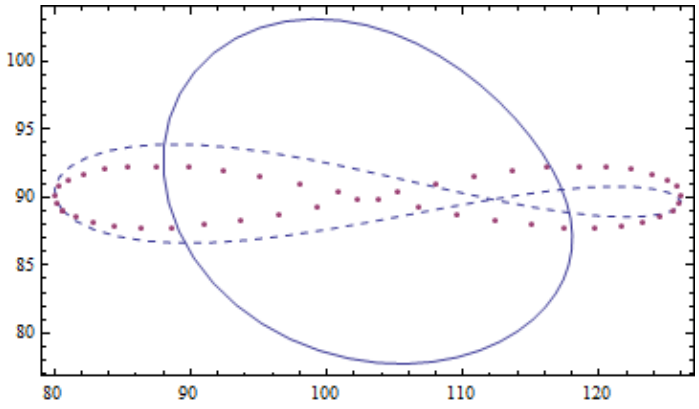

Figure 6: Track of Proxima on the western horizon, seen from the equator/terminator position. The dashed line is what we would see for a tidally locked earth. The dotted line applies to a circular earth orbit.

where σ is Stefan-Boltzmann's constant. With the size of Proxima and its temperature of 3000 K, $L = 1.7\%$ of the luminosity L_s of the sun. The stellar constant G_p at Atlantis relates to that of our sun G_s as

$$\frac{G_p}{G_s} = \frac{L d_s^2}{L_s d^2} = 0.72$$

The sun's solar constant on Earth's upper atmosphere is 1300 W/m^2. Atlantis receives 72% of that, $\sim$ 940 W/m^2 with a variation of $\pm 22\%$ due to the variation of distance during a Proxima year.

Atlantis

Atmosphere

Proxima Centauri is an M5 flare star (surface temperature 3000 K) with an intense X-ray and UV spectrum during its active periods. The upper atmospheric flux on Atlantis is about 870 W/m^2, equivalent to $\sim 60 - 70\,\%$ of the solar flux on Earth [21]. The strong X-ray and UV intensity counts only for $\sim 0.3\,W/m^2$ and is negligible for the total thermal input to Atlantis. The planet was assumed to have a strong magnetic field that protects the surface from stellar winds during the low activity of the star. During flares, superconducting coils serve as protecting shields against strong particle showers (see the section on magnetic shielding).

A basic problem is water trapping on the night side with km-thick ice sheets, depriving the planet of liquid water. This is expected for tidally locked planets with little water and a prevalence of continents on the night side. However, simulations show that a planet with continents and oceans like Earth develops a system of heat- and water circulation creating moderate climate conditions, especially close to the terminator [22].

Shielding: Magnetic fields

The magnetic field of the superconducting coils deflects the protons, creating a safe space. The calculation proceeds from the vector potential of a ring current I in spherical coordinates [23]

$$A_\varphi(r,\theta) = \frac{\mu_0}{4\pi}\frac{4Ia\left[(2-\kappa^2)K(\kappa^2)-2E(\kappa^2)\right]}{\kappa^2\sqrt{a^2+r^2+2ar\sin\theta}}$$

where E and K are elliptic integrals, a is the radius of the current loop, and $\mu_0 = 4\pi 10^{-7} H/m$ is the vacuum permeability. κ is a function of the dimensionless variable $\rho = r/a$,

$$\kappa^2 = \frac{4ar\sin\theta}{a^2+r^2+2ar\sin\theta} = \frac{4\rho\sin\theta}{1+\rho^2+2\rho\sin\theta}.$$

The magnetic field is

$$\vec{B} = \nabla \times \vec{A}.$$

The Lorentz force on a particle of charge e and relativistic mass m

$$\vec{F} = e\vec{v} \times \vec{B}$$

and Newtons second law lead to the differential equation

$$\ddot{\vec{r}} = \frac{e}{m}\dot{\vec{r}} \times \vec{B}$$

for the trajectory $\vec{r}(t)$, which can be solved with any symbolic solver such as Mathematica. In fact, protons are deviated from their otherwise straight trajectory. Those with impact parameter inside of the coil are mostly reflected, those outside of the coil are deflected. Only charged particles close to the axis will pass. Some trajectories are shown in Fig. 7.

The kinetic energy $mv^2/2$ and the angular momentum

$$L = mrv_\perp = \frac{mv_\perp^2}{\omega_c}$$

are conserved for motion of a charged particle in a magnetic field. Here r is the gyration radius, $v_\perp$ is the velocity component perpendicular to the magnetic field, and $\omega_c = qB/m$ is the cyclotron frequency of a particle with charge q and mass m. A particle crossing the axis of the loop under an angle θ at a distance z_{max} from the loop has $v_\perp = v\sin(\theta)$, and

$$L = \frac{m^2 v^2 \sin(\theta)^2}{qB_1}$$

where $B_1 = B_z(z_{max})$. The particle gyrates over the z-axis towards the loop, experiencing an ever increasing field $B(z)$. Now since L is conserved,

$$\frac{m^2 v^2 \sin(\theta)^2}{qB_1} = \frac{m^2 v_\perp(z)^2}{qB(z)} \leq \frac{m^2 v^2}{qB(z)}$$

which results in

$$\sin^2(\theta) \leq \frac{B_1}{B(z)}$$

because $v_\perp \leq v$. Particles starting under a larger angle to the field line are reflected before they reach z. This effect is known from magnetic bottles. The magnetic field compresses the ions towards the axis, but only a narrow bundle known as the *loss cone* in magnetic confinement [24] can pass the region with the strongest magnetic field in the center of the current loop. The rest is reflected and deviated from their straight path [25]. That said, the magnetic field of a ring coil (or a solenoid) is very efficient as a protective tool but cannot collect charged particles into a funnel such as the intake of a fusion chamber, over a large sweep area. Fishback [2] proposed a solution to the problem, exploiting a paraboloidal magnetic field. Closer scrutiny reveals that the proposal works in principle but suffers from the same problem of the very narrow loss cone. Scooping sufficient fuel with a Fishback field needs magnetic funnel lengths of $\gg 10^6$ km in flight direction [5].

Shielding: Mechanical support

The Lorentz force per volume — the force density — on the current carrying loop is

$$\frac{d\vec{F}}{dV} = \vec{j} \times \vec{B}.$$

Since B is predominantly in z direction, and $\vec{j}$ is tangent to the loop, the force density points radially outward. Writing

$$\frac{dF}{ds\,dA} = \frac{dI}{dA}B$$

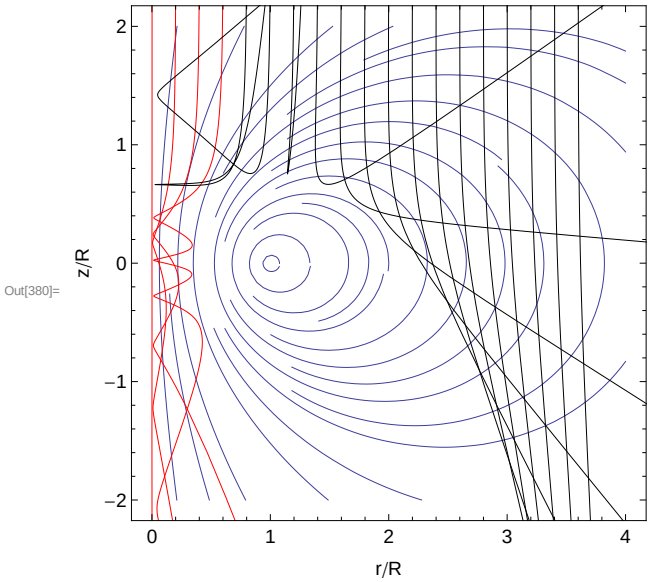

Figure 7: Some trajectories of 50 MeV-protons in the magnetic field of the big coil with radius 3 m and a central field strength of 2 T. The coil is at the origin, Protons enter from above. Scale in units of the ring radius. Only a small part of the protons would pass through the ring (red lines), spiralling down according to cyclotron gyration, the rest is deflected (black lines).

with the current I. The volume element on the wire is $dV = ds\,dA$ where ds is the line element along the wire, and dA is the surface element perpendicular to the line element. Assuming a cross section ΔA of the wire, within which the force density, the current density and the B field are approximately constant, the integral

$$\int_{\Delta A} \frac{dF}{ds\,dA}\,dA = \int_{\Delta A} \frac{dI}{dA} B\,dA$$

yields the surface tension of the loop:

$$\frac{dF}{ds} = I\,B.$$

The hoop stress, i.e. the tensile force on a cross section of the loop is the integral of the component of the surface tension which is perpendicular to the cross section, over half a loop of radius R:

$$F_t = \int_s \frac{dF_y}{ds}\,ds = RIB \int_0^\pi \sin(\phi)\,d\phi = 2RIB.$$

Thi is sketched in Fig. 8. For an order of magnitude estimate of the force we may take the expression of the B field in the center of the loop,

$$B_0 = \mu_0 \frac{I}{2R}$$

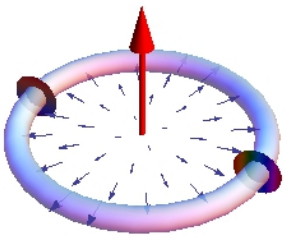

Figure 8: The mechanical support of a superconducting loop experiences a radial outward Lorentz force from the magnetic field (red arrow). The stress on the two cross sections is obtained from an integral over half a loop of the force component perpendicular to the cross sections.

which gives

$$F_t = \frac{(2R\,B_0)^2}{\mu_0}$$

where μ_0 is the magnetic permeability of vacuum. For the personal shields ($B_0 = 6$ T, $R = 0.3$ m) this gives a considerable tensile force of $\sim 10^7$ N. The mechanical support must sustain the tensile stress on the chosen cross section:

$$\sigma_{yy} = \frac{F_t}{2r^2\pi}$$

where r is the radius of a supporting rope or torus. The factor 2 in the denominator comes from the fact that in equilibrium, the outward force F_t acts on two cross sections of the ringlike support in the (x, z)-plane. We are thus looking for a material with high tensile strength and — for weight reasons — low density. For Kevlar, the above values stipulate a rope of 5 cm diameter which weighs ~ 6 kg.

The magnetic field at the wire itself is higher than our order of magnitude value B_0. Garren and Chen [26] give a correction factor of $\ln(8R/r) - 0.75$ for the force density at the loop which results in a thicker Kevlar rope weighing ~ 20 kg. I leave it to the educated reader to calculate the numbers for the big group shield, both for Kevlar and for a high strength steel.

Life forms

The energetic limit for splitting a water molecule - a main ingredient in photosynthesis - is 1.23 eV, corresponding to a wavelength of 1000 nm. But plant leafs on Earth reflect infrared radiation with wave length > 700 nm. If this limit were pushed into the near infrared region, a larger portion of the star's spectrum could be used [27]. It is known that some cyanobacteria utilize a different phytosynthesis cycle with lower photon energy. A similar mechanism was assumed to be at work on Atlantis. Still, the lower photonic influx and the less effective photosynthesis leads to slower growth of plants, resembling the vegetation on Earth at high latitudes.

The strong X-ray and UV spectrum during stellar flares, up to 200 times higher than on Earth, poses a problem for plant survival. It is planned to insert the gene sequence RADPR coding for the rapid repair mechanism identified in *Deinococcus radiodurans* [28] - a bacterium that supports 10^4 Gray, a dose more than thousand times higher than a human being could sustain - into herbal life forms.

Acknowledgments

Many thanks to my colleagues Pascal Bernaud and Ann-Lenaig Hamon from CentraleSupélec in Paris and Cécile Hébert from the École Polytechnique Fédérale de Lausanne for their careful calculations, as well as to the students of the lectures on *How physics inspires SciFi* in Vienna, Paris and Beijing, who critically questioned many texts and gained surprising insights that the lecturers had missed. My special thanks go to Herbert W. Franke for valuable comments and to my critical test readers Brandon Weigel, Herbert "Hörby" Hutter and Albert Blauensteiner, who discovered a great deal of nonsense. Paul Gilster's detailed knowledge of the physics of Bussard ramjets was extremely helpful.

References

[1] R. W. Bussard, Galactic matter and interstellar flight, Astronauica Acta 6 (4) (1960).

[2] J. F. Fishback, Relativistic interstellar spaceflight, Astronautica Acta 15 (1) (1969) 25–35.

[3] C. Semay, B. Silvestre-Brac, The equation of motion of an interstellar Bussard ramjet, European Journal of Physics 26 (1) (2005) 75–83.

[4] O. G. Semyonov, Radiation hazard of relativistic interstellar flight, Acta Astronautica 64 (5-6) (2009) 644–653.

[5] P. Schattschneider, Notes on the Fishback Ramjet, unpublished.

[6] G. H. Gillespie, Systematics of electron-stripping cross sections for fast hydrogenic ions penetrating solids, Nuclear Inst.and Methods in Physics Research, B 2 (1-3) (1984) 231–234.

[7] K. von Reden, M. Zhang, M. Meigs, E. Sichel, S. Fang, R. H. Baughman, Carbon nanotube foils for electron stripping in tandem accelerators, Nuclear Instruments and Methods in Physics Research, Section B: Beam Interactions with Materials and Atoms 261 (1-2 SPEC. ISS.) (2007) 44–48.

[8] M. B. Smirnov, V. P. Kraĭnov, Critical fields for ionization of the hydrogen molecule and the molecular hydrogen ion, Journal of Experimental and Theoretical Physics 85 (3) (1997) 447–450.

[9] D. P. Whitmire, Relativistic spaceflight and the catalytic nuclear ramjet, Acta Astronautica 2 (1975) 497–509.

[10] H. A. Bethe, Energy production in stars, Phys. Rev. 55 (1939) 434–456. doi:10.1103/PhysRev.55.434.
URL https://link.aps.org/doi/10.1103/PhysRev.55.434

[11] A. Einstein, Zur Elektrodynamik bewegter Körper, Annalen der Physik 17 (4) (1905) 891–921.

[12] R. Klauber, Relativistic rotation: A comparison of theories, Foundations of Physics 37 (2007) 198–252.

[13] M. Yahalomi, Measurement of the time dilation in rotational movements, Foundations of Physics Letters 10 (2002) 495.

[14] N. Sama, On the Ehrenfest paradox, American Journal of Physics 40 (1972) 415–418.

[15] A.-L. Hamon, D. Aubry, private communication (2020).

[16] https://physics.nist.gov/cgi-bin/Star/ap_table.pl.

[17] https://www.youtube.com/watch?v=o4ZqfEJTGzw,citedbyhttps://de.wikipedia.org/wiki/Railgun.

[18] https://en.wikipedia.org/wiki/Relativisticaberration.

[19] J. Terrell, Invisibility of the Lorentz contraction, Physical Review 116 (1959) 1041–1045.

[20] https://en.wikipedia.org/wiki/Kepler.

[21] I. Ribas, M. D. Gregg, T. S. Boyajian, E. Bolmont, The full spectral radiative properties of Proxima Centauri, Astronomy and Astrophysics 603 (2017) A58.

[22] J. Yang, Y. Liu, Y. Hu, D. S. Abbot, Water trapping on tidally locked terrestrial planets requires special conditions, Astrophysical Journal Letters 796 (2) (2014).

[23] J. Simpson, Simple analytic expressions for the magnetic field of a circular current loop, https://ntrs.nasa.gov/search.jsp?R=20010038494 (2001).

[24] P. T. Gallagher, Introduction to plasma physics, Website (2005).

[25] C. Gros, Universal scaling relation for magnetic sails: momentum braking in the limit of dilute interstellar media, J. Physics Comm. 1 (045007) (2017).

[26] D. A. Garren, J. Chen, Lorentz self-forces on curved current loops, Physics of Plasmas 1 (10) (1994) 3425–3436.

[27] J. Gale, A. Wandel, The potential of planets orbiting red dwarf stars to support oxygenic photosynthesis and complex life, International Journal of Astrobiology 16 (1) (2016) 1–9.

[28] Y. Kawaguchi, M. Shibuya, I. Kinoshita, J. Yatabe, I. Narumi, H. Shibata, R. Hayashi, D. Fujiwara, Y. Murano, H. Hashimoto, E. Imai, S. Kodaira, Y. Uchihori, K. Nakagawa, H. Mita, S.-i. Yokobori, A. Yamagishi, DNA damage and survival time course of deinococcal cell pellets during 3 years of exposure to outer space, Frontiers in Microbiology 11 (2020) 2050.